NeuroImage 310 (2025) 121165

Contents lists available at ScienceDirect

NeuroImage

journal homepage: www.elsevier.com/locate/ynimg

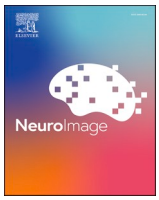

Fibrillar amyloidosis and synaptic vesicle protein expression progress jointly in the cortex of a mouse model with β-amyloid pathology

L.H. Kunze [a,b], G. Palumbo [a], J. Gnörich [a,b], K. Wind-Mark [a], R. Schaefer [a], S. Lindner [a], F.-J. Gildehaus [a], S. Ziegler [a,c], M. Brendel [a,b,d,*]

[a] Department of Nuclear Medicine, University Hospital, LMU Munich, Munich, Germany
[b] German Center for Neurodegenerative Diseases (DZNE) Munich, Munich, Germany
[c] Department of Nuclear Medicine, Hannover Medical School (MHH), Hannover, Germany
[d] Munich Cluster for Systems Neurology (SyNergy), Ludwig Maximilian University of Munich, 81377 Munich, Germany

ARTICLE INFO

Keywords:
Synaptic density
Alzheimer's disease
SV2A-PET
β-amyloid

ABSTRACT

Neurodegeneration, accumulation of β-amyloid (Aβ) plaques, and neuroinflammation are the major hallmarks of Alzheimer's disease. Here, we aimed to investigate the temporal and spatial association between synaptic activity, Aβ plaque load, and neuroinflammation in an Aβ mouse model with limited neurodegeneration.

26 APPSL70 and 15 C57Bl/6 mice underwent longitudinal PET-scans with [^{18}F]UCB-H from plaque onset to levels of strong plaque load (5.3 - 11.0 months of age) to assess the synaptic vesicle protein 2A (SV2A) expression, [^{18}F]FBB to determine the fibrillar Aβ plaque load, and [^{18}F]GE-180 and [^{18}F]F-DED to assess microglial and astroglial (re)activity. Statistical parametric mapping was performed to uncover similarities between the binding patterns of all four tracers.

We found a continuous increase in Aβ-PET in APPSL70 mice from 5.3 to 11.0 months of age, resulting in a significantly higher [^{18}F]FBB PET signal in the cortex, hippocampus, and thalamus of APPSL70 mice compared to C57Bl/6 mice at 11.0 months of age. Parallel increases in SV2A-PET signals were observed in the cortex and thalamus of APPSL70 mice compared to C57Bl/6 mice. Statistical parametric mapping revealed a similar pattern of Aβ- and SV2A-PET differences (dice coefficient 53 %). Patterns of microglia activation showed stronger congruency with SV2A expression (dice coefficient 58 %) than patterns of reactive astrogliosis (dice coefficient 26 %).

APPSL70 mice with limited neurodegeneration comprise a close temporal and spatial association between SV2A expression, Aβ plaque load, and microglial activation. SV2A PET imaging in APPSL70 mice may facilitate longitudinal monitoring of increased synaptic activity in the earliest phase of AD.

1. Introduction

Alzheimer's disease (AD) is a multifactorial disorder ultimately leading to neurodegeneration (De Wilde et al., 2016; Mecca et al., 2020; Terry et al., 1991; Wolfe, 2021). Pathological changes on the cellular level can be observed years before the onset of clinical symptoms, with the accumulation of β-amyloid (Aβ) being one of the earliest pathological changes in brain (Jack et al., 2010; Lichtenthaler, 2017; Wolfe, 2021). These protein aggregates arise by a disturbed processing of the amyloid precursor protein (APP) by the γ-secretase. This enzyme cleaves the APP into fragments of different lengths with longer fragments being more prone to aggregate into Aβ-plaques (Haapasalo and Kovacs, 2011; Voytyuk et al., 2018), which also trigger inflammatory processes (Fakhoury, 2018; S. E. Hickman et al., 2008; Wolf et al., 2017). While microglial activation and astrocytic reactivity can have positive effects, namely the dealing with pathogens and the clearing of cellular debris and pathological protein aggregation (Acioglu et al., 2021; Bolós et al., 2015; Ewers et al., 2020; Fakhoury, 2018; Olsen et al., 2018; Spanos and Liddelow, 2020; Wolf et al., 2017), chronic inflammation has been shown to have detrimental effects on the surrounding tissue (Eckenweber et al., 2020; Fakhoury, 2018; Hickman et al., 2018). Moreover, as astrocytes are also involved in multiple other functions, like setting up the blood-brain barrier and nourishing neurons (Acioglu et al., 2021; Fakhoury, 2018; Olsen et al., 2018; Spanos and Liddelow,

* Corresponding author at: Department of Nuclear Medicine, University Hospital, LMU Munich, Marchioninistr. 15, 81377 Munich, Germany.
E-mail address: matthias.brendel@med.uni-muenchen.de (M. Brendel).

https://doi.org/10.1016/j.neuroimage.2025.121165
Received 17 December 2024; Received in revised form 13 February 2025; Accepted 19 March 2025
Available online 20 March 2025

2020), their reactivity leads, amongst others, to a decreased synaptic inhibition. Another factor that seems to be involved in the dysregulation of synaptic signaling are the synaptic vesicle glycoproteins 2 (SV2), as they are involved in the fusion of synaptic vesicles and possibly also in Ca^{2+} dynamics (Janz et al., 1999; Rossi et al., 2022; Xu and Bajjalieh, 2001). Especially SV2A is crucial for survival and deletions can lead to severe seizures, possibly by an imbalance of excitatory and inhibitory neuronal activity (Janz et al., 1999). This is in concordance with an observed neuronal hyperexcitability in AD patients at early stages of the disease and models at early and even presymptomatic stages, especially in proximity to Aβ plaques (Busche et al., 2008; Sha et al., 2023; Targa Dias Anastacio et al., 2022). A longitudinal assessment of synaptic activity, e.g. by the use of SV2A-PET, could be beneficial for an early identification of a disrupted neuronal signaling. A suitable PET tracer targeting SV2A is [^{18}F]UCB-H, its structure deriving from the anti-epileptic drug levetiracetam and shown to reliably bind to SV2A. Thus, this tracer provides a rather direct read-out of synaptic density/activity (Bastin et al., 2020; Bretin et al., 2013, 2015; Serrano et al., 2019; Vogler et al., 2023; Warnock et al., 2014) compared to the gold-standard [^{18}F]fluordesoxyglucose ([^{18}F]FDG) measurements of neurodegeneration, that is compiled of neuronal and glial glucose uptake, however (Bartos et al., 2024). Mouse models of AD provide valuable insights into the disease, aiding to a better understanding of the pathological mechanisms within an organism. With a wide variety of techniques to investigate alterations in these mouse models, preclinical PET has the advantage to follow up on the pathological changes within the same animal longitudinally, thereby also reducing the number of animals needed for each study (Palumbo et al., 2023). Thus, in this study, we aimed to investigate the connection between Aβ aggregation, neuroinflammation, and synaptic density/activity. Therefore, we performed longitudinal PET-scans at 5.3, 8.9, and 11.0 months of age on APPSL70 mice and age-matched wild-type controls with [^{18}F]florbetaben ([^{18}F]FBB) to target the Aβ plaques, [^{18}F]GE-180 to target activated microglia, [^{18}F]F-DED to target reactive astrocytes, and [^{18}F]UCB-H to assess the synaptic activity/density. In addition, we assessed the spatial distribution pattern of the respective tracers and examined their similarity by performing a statistical parametric mapping and calculating a dice coefficient.

2. Materials and methods

2.1. Animals and study design

All experiments were carried out in compliance with the National Guidelines for Animal Protection, Germany, and with the approval of the regional animal care committee (Regierung von Oberbayern) and were overseen by a veterinarian. The experiments complied with the ARRIVE guidelines and were carried out in accordance with the U.K. Animals (Scientific Procedures) Act, 1986 and associated guidelines, EU Directive 2010/63/EU for animal experiments. Animals were housed in a temperature- and humidity-controlled environment with a 12 h light-dark cycle, with free access to food and water.

APPSL70 mice were generated on a C57BL/6 background carrying the Swedish (K670N/M671 L) and London (V717I) mutation under the control of the *thy1* promotor. In these mice, the first fibrillary Aβ deposits occur at 2.5 months of age and is thus similar to a mouse line published by Blanchard et al. (2003). Aβ40 and Aβ42 protein levels rise exponentially starting from three months of age and result in measurable Aβ-PET signals from 5 to 6 month of age (Blume et al., 2018; Sacher et al., 2020).

28 APPSL70 and 17 C57Bl/6 mice underwent a longitudinal multitracer PET-study as described in Table 1. Variability in the group sizes are due to methodological variations, which include technical problems in the acquisition of the scan or an insufficient amount of injected activity for few mice. These data points were excluded from the analysis, however, other sufficient data points from the same animal were kept within the analysis. After the second follow-up scan (Follow-up 2), mice were transcardially perfused with PBS. Brains were harvested and one hemisphere was fixed in 4 % paraformaldehyde for immunohistochemical analyses.

Table 1
Number (N) of successful [^{18}F]FBB (Aβ), [^{18}F]UCB-H (SV2A), [^{18}F]F-DED (MAO-B), and [^{18}F]GE-180 (TSPO) PET-scans.

	Baseline		Follow-up 1		Follow-up 2	
	5.3 months of age		8.9 months of age		11.0 months of age	
	C57Bl/6	APPSL70	C57Bl/6	APPSL70	C57Bl/6	APPSL70
[^{18}F] FBB	$N = 17$	$N = 28$	$N = 14$	$\mathbf{N = 25}$	$N = 14$	$N = 26$
[^{18}F] UCB-H	$N = 16$	$N = 19$	$N = 16$	$N = 26$	$N = 15$	$N = 26$
[^{18}F] F-DED	$N = 17$	$N = 27$	$N = 14$	$N = 26$	$N = 14$	$N = 26$
[^{18}F] GE-180	$N = 17$	$N = 27$	$N = 16$	$N = 24$	$N = 14$	$N = 25$

2.2. PET imaging

PET-tracer radiochemistry, PET image acquisition, and image preprocessing were performed as described previously (Ballweg et al., 2023; Brendel et al., 2016; Overhoff et al., 2016; Vogler et al., 2023). In brief, mice anesthetized with isoflurane underwent four different PET scans on three consecutive timepoints. Therefore, they were injected an average dose of 15.2 ± 1.6 MBq of [^{18}F]UCB-H, 14.0 ± 3.2 MBq of [^{18}F]FBB, 10.3 ± 3.6 MBq of [^{18}F]F-DED, and 13.8 ± 2.7 MBq of [^{18}F]GE-180. In between the PET-scans on each timepoint, mice were resting for at least two days. For each PET-scan, four mice were scanned simultaneously and irrespective of their genotype in a randomized way in the MediSoNanoScan PET-CT with a dynamic 60 min emission recording for [^{18}F]UCB-H, and static 30–60 min p.i. imaging windows for [^{18}F]FBB and [^{18}F]F-DED, as well as 60–90 min p.i. in the case of [^{18}F]GE-180.

2.3. PET image analysis

All image analysis were performed using PMOD (version 3.5, PMOD Technologies, Zurich, Switzerland) as described earlier (Overhoff et al., 2016). In brief, images were spatially normalized to a template and subsequently adjusted to the tracer uptake in the hypothalamus by calculating a standardized uptake value ratio (SUVr). The hypothalamus (11 mm^3) was chosen as a uniform reference region since there were no significant differences in [^{18}F]UCB-H V_T or SUV of [^{18}F]FBB, [^{18}F]GE-180 and [^{18}F]F-DED between C57Bl/6 and APPSL70 mice (see results section). Cortex (146 mm^3), hippocampus (24 mm^3), and thalamus (27 mm^3) served as target regions as they comprise Aβ rich regions in APPSL70 mice (Blume et al., 2018; Sacher et al., 2020). The respective volumes of interests were retrieved from the Mirrione Atlas. The midbrain (3 mm^3), being clinically affected later by Aβ accumulation (Hampel et al., 2021), was chosen as amyloid negative control region. To avoid spill-in effects from regions highly affected by group level differences, the midbrain region was defined manually by placing a suitable sphere within this anatomical region.

To validate the SUVr analysis, we performed an additional analysis for [^{18}F]UCB-H with a tissue independent normalization method. [^{18}F]UCB-H volume-of-distribution (V_T) images were calculated with an image derived input function (IDIF) following the methodology described by Logan et al. implemented in PMOD (Logan et al., 1990). To obtain the blood curve, a spherical VOI with a radius of 2.5 mm was placed in the heart. For modelling of the dynamic imaging data, the deviation of the data points to the regression line (maximum error) was less than 10 % and a V_T threshold of 0 % were applied, retaining all of

the pixels.

Statistical parametric mapping (SPM) and Dice coefficient analysis was applied as described previously (Gnörich et al., 2024). In brief, SPM was performed in Matlab (*MATLAB*, 2016) with SPM12 (*SPM12*, 2016) by calculating a two-sample *t*-test between APPSL70 and C57Bl/6 mice to compare the tracer distribution patterns of both groups. Next, we binarized the map of each tracer using the respective t-values obtained from SPM and calculated the dice coefficients between each tracer to assess the similarity in their group differences (Förster et al., 2012; Zou et al., 2004) with a publically available Matlab script (https://github.com/rordenlab/spmScripts/blob/master/nii_dice.m).

2.4. Immunohistochemistry

Immunohistochemistry was performed to assess SV2A expression levels. To this end, paraformaldehyde-fixed 50 μm sagittal brain sections were incubated overnight at 4 °C in PBS with 5 % normal goat serum containing chicken polyclonal anti-NeuN primary antibody (1:500, Sigma-Aldrich, St. Louis, MO, USA, ABN91), rabbit polyclonal anti-SV2A primary antibody (1:500, Synaptic Systems GmbH, Göttingen, Germany, 119 002), and mouse monoclonal anti-β amyloid primary antibody (NAB228, 1:500, Santa Cruz Biotechnology, Dallas, TX, USA, sc-32,277). Afterwards, slices were incubated for 2 h at room temperature with a suitable secondary antibody. Imaging was performed on the THUNDER Imager Tissue (Leica Microsystems CMS GmbH, Wetzlar, Germany) with a x63 objective in two sagittal sections per animal. Target area was the cortex where six images per slice distributed equally across the frontal and posterior cortical areas were acquired. Images were processed with the LAS X Software (version 3.9.1.28433) and image analysis was performed on 16-bit images with ImageJ (version 1.54f) (Schindelin et al., 2012) by quantifying the area above a threshold of 35 for SV2A within the NeuN+ area. NAB228 was interpreted qualitatively.

2.5. Statistics

Group differences between genotype in longitudinal PET-data were assessed with a mixed-effects model and Tukey's multiple comparisons test using GraphPad Prism statistical software (version 9.5.1 for Windows, GraphPad Software, San Diego, CA, USA). For immunohistochemical data, outliers were considered values that were 1.5 IQR above the 75 %- or below the 25 %-quartile. Moreover, values that were below the negative control were excluded from the analysis. From the remaining values, the mean was calculated to obtain one value for each mouse. An unpaired *t*-test was applied to uncover differences between genotypes for SV2A in NeuN+ area with GraphPad Prism statistical software (version 9.5.1 for Windows, GraphPad Software, San Diego, CA, USA). A threshold of $p < 0.05$ was considered significant to reject the null hypothesis.

3. Results

3.1. Hypothalamus is a suitable joint reference region for multitarget PET imaging with [^{18}F]UCB-H, [^{18}F]FBB, [^{18}F]F-DED, and [^{18}F]GE-180 in the comparison of APPSL70 an C57Bl/6 mice

First, we aimed to find a uniform reference region for all four tracers used in this study. Comparing the hypothalamic PET signal of APPSL70 and C57Bl/6 mice at 11.0 months of age for [^{18}F]UCB-H, [^{18}F]FBB, [^{18}F]F-DED, and [^{18}F]GE-180, respectively, we found no significant differences between these two groups (**Supplementary Table 1, Supplementary Figure 1**). Thus, we decided that the hypothalamus is a suitable uniform reference region that can be used to normalize the PET signal for all four tracers.

3.2. [^{18}F]UCB-H pet signal increases during aging in APPSL70 mice compared to C57Bl/6 controls

Mixed effect model analysis revealed significant SUVr differences between APPSL70 and C57Bl/6 mice in the SV2A PET signal at 11.0 months of age (cortex: $p = 0.023$, thalamus: $p = 0.032$). For the hippocampus, there was a trend to significance for 11.0 months of age ($p = 0.061$). Moreover, a significant drop of SV2A SUVr from 5.3 to 11.0 months of age could be observed in C57Bl/6 mice in the cortex ($p = 0.002$), hippocampus ($p = 0.0005$), and thalamus ($p = 0.002$), and in APPSL70 mice in the hippocampus ($p = 0.002$) and thalamus ($p = 0.034$). After conversion of differences between APPSL70 and C57Bl/6 mice into z-scores, the SV2A PET signal of APPSL70 mice was significantly higher in the cortex at 8.9 ($p = 0.017$) and 11.0 ($p = 0.023$) months of age as well as in the thalamus of 8.9 ($p = 0.029$) and 11.0 ($p = 0.032$) months of age (Fig. 1). As synaptic changes could constitute a global phenomenon, we aimed to perform a tissue independent analysis to confirm the SUVr results. Thus, a validation analysis was performed with SV2A distribution volume images (V_T) to exclude cerebral blood flow as a driver of SV2A PET changes. A similar consistently rising pattern for SV2A PET V_T z-scores of APPSL70 mice compared to C57Bl/6 controls was observed, which correlated strongly with SUVr at the individual level in the cortex ($r = 0.75$, $p < 0.0001$), hippocampus ($r = 0.63$, $p < 0.0001$), and thalamus ($r = 0.68$, $p < 0.0001$). SV2A-PET V_T were significantly increased in the cortex considering only the last timepoint at 11.0 months of age ($p = 0.031$, Mann-Whitney-test), but showed lower effect size (Cohens $d = 0.62$ for V_T vs $d = 1.02$ for SUVr) compared to SUVr due to the higher variance in IDIF-based V_T computation.

3.3. Spatio-temporal agreement between changes in SV2A expression and fibrillary amyloidosis in APPSL70 compared to C57Bl/6 mice

For [^{18}F]FBB PET signals as an index of fibrillar amyloidosis, we found a significant rise in APPSL70 mice compared to C57Bl/6 controls in the cortex from 8.9 to 11.0 months of age ($p = 0.002$), as well as significant differences between APPSL70 and C57Bl/6 mice at 11.0 months of age (cortex and hippocampus: $p < 0.0001$, thalamus: $p = 0.0007$).

Comparison of the distribution of [^{18}F]FBB and [^{18}F]UCB-H with statistical parametric mapping revealed similar regional group differences for Aβ and SV2A**.** Both tracers showed differences in 11.0 months old APPSL70 and C57Bl/6 mice predominantly in the cortex. The similarity of the tracer-specific group differences was assessed with the dice coefficient, showing a 53 % similarity for Aβ and SV2A (Fig. 2). Since the midbrain is a region that is usually affected late by Aβ plaques (Hampel et al., 2021), it served as a negative control and revealed no significant differences in neither [^{18}F]FBB nor [^{18}F]UCB-H PET signal between APPSL70 and C57Bl/6 mice (**Supplementary Figure 2**).

3.4. Microglial activation shows more spatio-temporal coupling with SV2A expression than astroglial reactivity

The TSPO PET signal as an index of microglial activation increased significantly in APPSL70 mice from 5.3 to 8.9 months of age in the cortex ($p < 0.0001$), hippocampus ($p = 0.0007$), and thalamus ($p = 0.027$), and from 5.3 to 11.0 months of age ($p < 0.0001$ in all three brain regions). In addition, APPSL70 mice had a significantly higher TSPO PET signal compared to C57Bl/6 controls at 8.9 months of age in the cortex ($p = 0.018$) and at 11.0 months of age in the cortex ($p = 0.0005$) and hippocampus ($p < 0.0001$). While astrocytic reactivity significantly decreased in C57Bl/6 mice from 8.9 to 11.0 months of age in the cortex ($p = 0.046$), hippocampus ($p = 0.019$), and thalamus ($p = 0.042$), MAO-B PET signals significantly increased in the thalamus in 11.0 month old APPSL70 mice compared to C57Bl/6 controls ($p = 0.029$). The dice coefficient indicated a similarity of the tracer-specific group differences

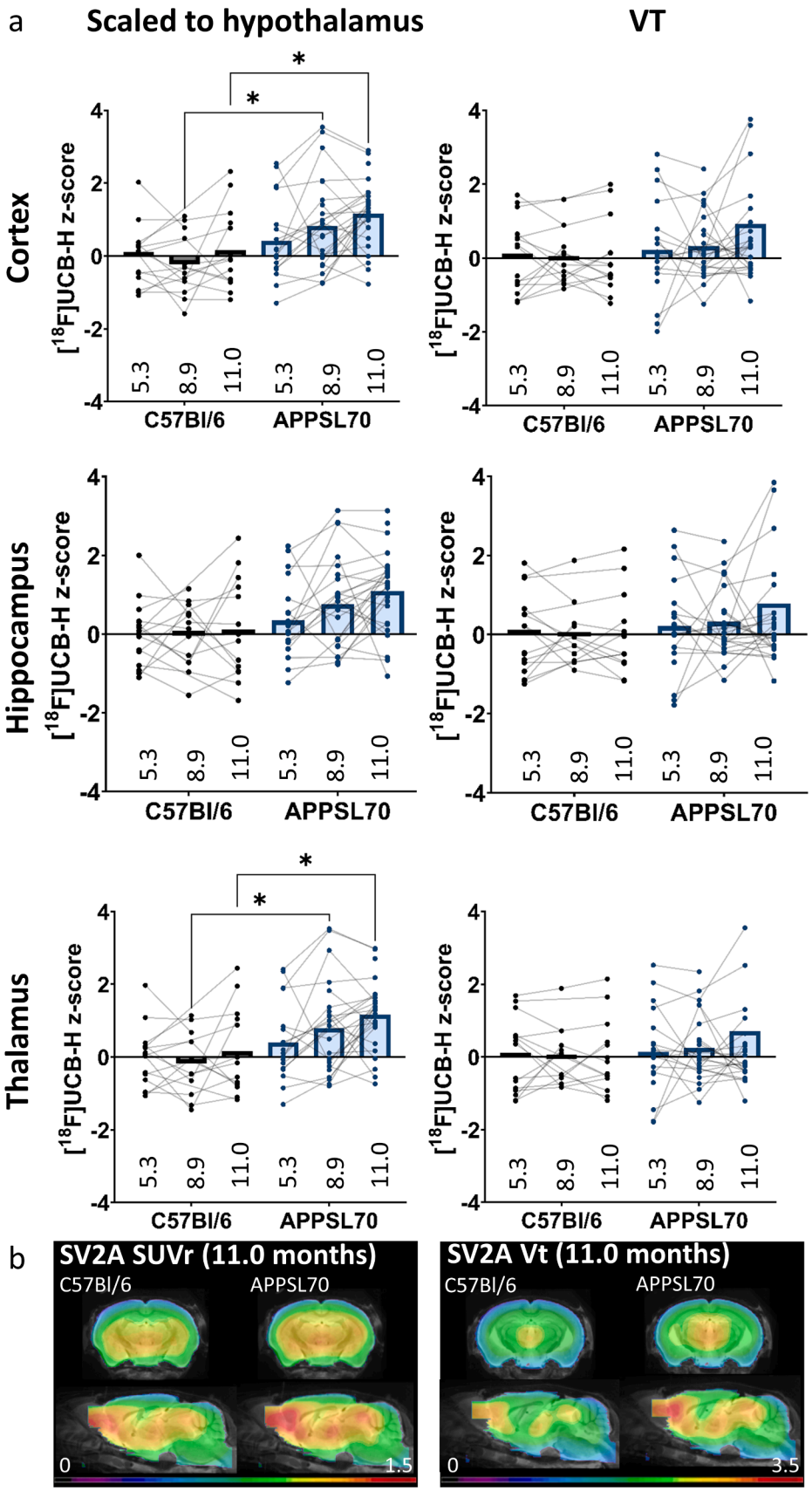

Fig. 1. (a) SUVr z-scores of SV2A PET signal of C57Bl/6 and APPSL70 mice scaled to hypothalamus as well as V_T z-scores of SV2A PET data of C57Bl/6 and APPSL70 mice at 5.3, 8.9, and 11.0 months of age. (b) Average-images of SUVr- and V_T-scaled SV2A PET data of 11 months old C57Bl/6 and APPSL70 mice.

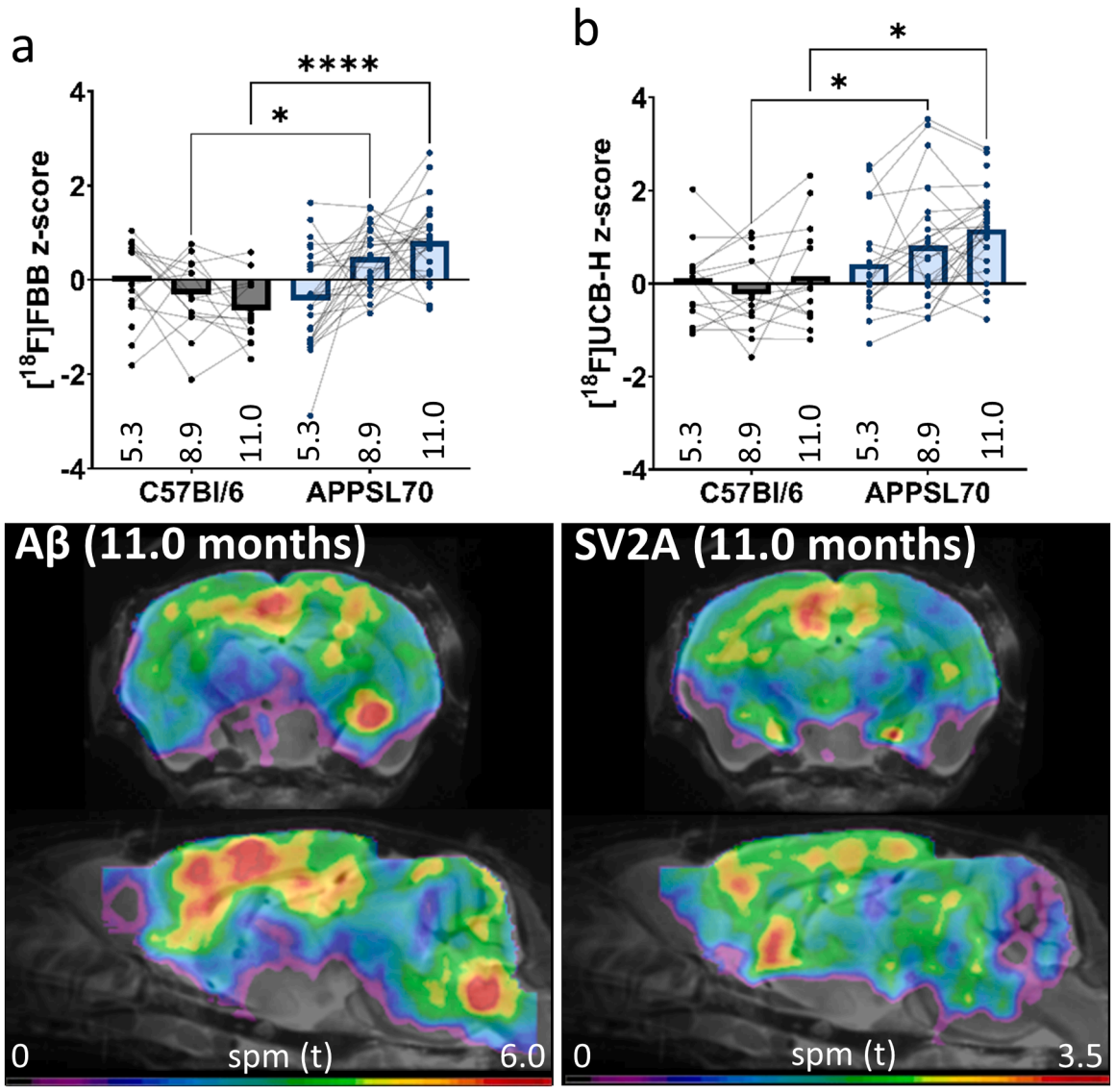

Fig. 2. Statistically significant group differences calculated by statistical parametric mapping for Aβ (a) and SV2A (b) between 11.0 months old C57Bl/6 and APPSL70 mice with the respective z-scores of the cortex at 5.3, 8.9, and 11.0 months of age.

of 58 % for TSPO and SV2A, and 64 % for TSPO and Aβ. In contrast, MAO-B group differences were less similar to Aβ (35 %), SV2A (26 %), and TSPO (35 %) (Fig. 3), mainly driven by the overlap in the thalamus but distinct in the cortex and the brainstem.

3.5. Significantly higher SV2A expression levels in neurons of APPSL70 mice compared to C57Bl/6 controls

The immunohistochemical staining of synaptic density revealed significantly higher levels of SV2A+ area in NeuN+ area in APPSL70 mice compared to C57Bl/6 controls ($p = 0.033$, Fig. 4). This finding was in accordance to the [^{18}F]UCB-H PET results reported above, also showing a trend towards correlation between the immunohistochemical results and the [^{18}F]UCB-H PET signal ($R^2 = 0.083$, $p = 0.193$).

4. Discussion

We present the first multiple-tracer longitudinal study describing the association of Aβ plaque deposition, SV2A expression levels, and neuroinflammation in a mouse model of Alzheimer's disease with limited neurodegeneration. We found significantly higher widespread fibrillar amyloidosis, as well as a significantly higher microglial activation in the cortex and hippocampus of 12-month-old APPSL70 mice compared to age-matched C57Bl/6 controls, showing the progressing amyloid-pathology in APPSL70 mice as previously described (Blume et al., 2018). Moreover, we observed a significant subcortical astrogliosis as measured by significantly higher [^{18}F]F-DED PET signal in the thalamus of 11 months old APPSL70 mice compared to age-matched C57Bl/6 controls.

Furthermore, we saw a significant drop in synaptic activity in the hippocampus and thalamus of APPSL70 mice from 5.3 to 11.0 months of age. This decrease was also found in C57Bl/6 mice and is for the C57Bl/6 mice most likely part of a normal aging process (Cizeron et al., 2020). In addition, the synaptic activity was significantly higher in the cortex and thalamus of 11 months old APPSL70 mice compared to age-matched C57Bl/6 controls, as also confirmed in the immunohistochemical analysis. A limiting factor is the missing significant correlation between SV2A quantification in PET and immunohistochemistry on an individual level. However, such a correlation is challenging due to the difficult quantification of the fine structured synapses. Thus, our trend to correlation is already encouraging.

The observed rise in SV2A expression levels might be

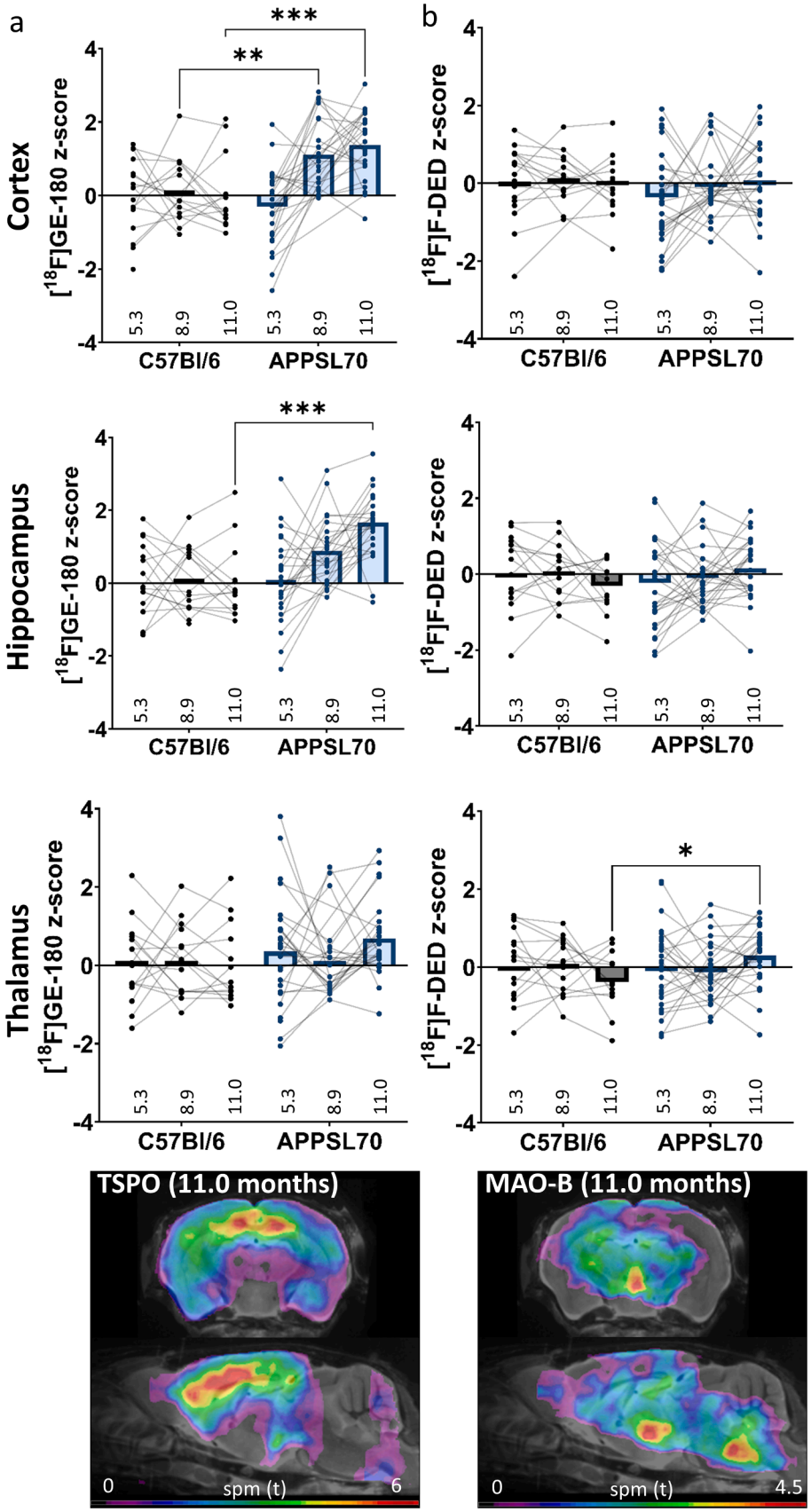

Fig. 3. Statistically significant group differences calculated by statistical parametric mapping for TSPO (a) and MAO-B (b) between 11.0 months old C57Bl/6 and APPSL70 mice with the respective z-scores of the cortex, hippocampus, and thalamus at 5.3, 8.9, and 11.0 months of age.

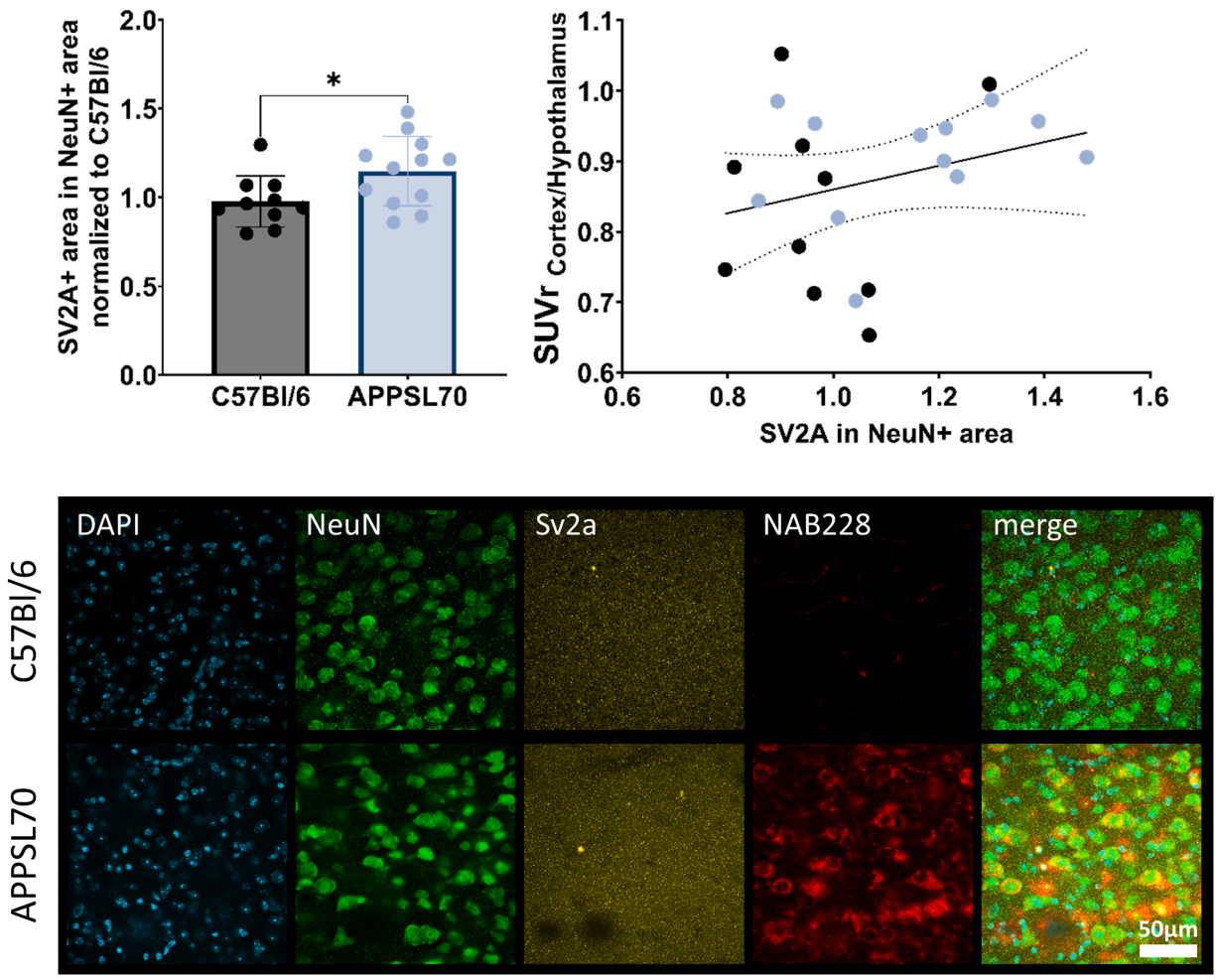

Fig. 4. Immunohistochemical analysis of SV2A expression levels in the frontal cortex of APPSL70 mice and C57Bl/6 controls together with representative maximum projections of immunohistochemical stainings in the frontal cortex.

counterintuitive at first, as a wide variety of studies showed a general decline of synapses and SV2A in Alzheimer's disease patients (Bastin et al., 2020; Chen et al., 2018; Mecca et al., 2020; Terry et al., 1991), also measured as cerebral energy consumption as indirect read-out by [^{18}F]FDG PET (Bateman et al., 2012; Benzinger et al., 2013; Iaccarino et al., 2024). However, it was also shown that a hypermetabolism could be observed in asymptomatic patients (i.e. mutation carriers of genetically determined AD) and patients with only subtle changes of cognition early in the disease (Bakhtiari et al., 2023; Benzinger et al., 2013). In addition, hypermetabolism could also be observed in amyloidosis mouse models in [^{18}F]FDG-PET (Ruch et al., 2024). Thereby, limited neurodegeneration in Aβ mouse models and APPSL70 in particular needs to be considered. Thus, the used Aβ mouse model offers the potential to study specific features in the temporal progression of the disease, i.e. the phase of Aβ build-up where no tau aggregates and neurodegeneration are present yet (A+T-N-). While an increased cerebral glucose uptake can also be influenced by neuroinflammation (Bartos et al., 2024; Gnörich et al., 2023; Ruch et al., 2024), SV2A-PET provides an unbiased read-out of synaptic density/activity. Our study aimed to test the translational ability to monitor increased synaptic activity during amyloid build-up, but we cannot shed light onto the mechanisms, which poses a limitation to this study. In principle, there are two possible explanations for the observed difference in SV2A expression levels measured by [^{18}F]UCB-H PET signal and immunohistochemical stainings of SV2A of APPSL70 mice compared to C57Bl/6 controls: First, SV2 was found to be located in dystrophic neurites (Snow et al., 1996), pointing to the possibility that the PET signal increased due to an increase in dystrophic neurites and thus a dysregulated synaptic expression. Nevertheless, SV2 expression was still lower in Alzheimer's disease patients compared to cognitively normal controls despite an abundance of Aβ and dystrophic neurites (Snow et al., 1996). Thus, the more probable second explanation could be a compensatory increase in synaptic density when neurodegeneration is starting. Bell et al. (2003) found an elevation in synaptic density for glutamatergic and GABAergic neurons before a measurable neurodegeneration in TgCRND8 mice. Moreover, an increased presynaptic bouton density was found for glutamatergic neurons and the authors suggest an underlying compensatory mechanism counteracting the Aβ-induced disturbed synaptic signaling (Bell et al., 2007). Possibly, this increase in synaptic density might add to an increased signaling capacity and thus lead to the described hyperexcitability of neurons in Alzheimer's disease, which was found to be closely connected to the Aβ plaques (Busche et al., 2008; Targa Dias Anastacio et al., 2022). In addition, we discovered a close similarity to respective group differences between APPSL70 and C57Bl/6 mice for [^{18}F]FBB and [^{18}F]UCB-H, supporting the hypothesis that an increase in synaptic density is most likely a compensatory mechanism induced by Aβ plaque deposition and preceding neurodegeneration and also possibly increasing the pathological features (Targa Dias Anastacio et al., 2022).

In addition, both fibrillar amyloidosis and SV2A expression showed a high spatio-temporal agreement with microglial activity. As shown previously, there is a close connection between microglial activation and Aβ deposition in different mouse models of amyloidosis (Blume et al., 2018; Brendel et al., 2016; Sacher et al., 2020), with a strong early increase in microglial activation (Blume et al., 2018). The microglial

activation with increased release of proinflammatory cytokines might again add to a neuronal hyperexcitability (Busche et al., 2008; Targa Dias Anastacio et al., 2022), possibly explaining an increased density of SV2A PET signal. However, this hypothesis would need further investigation including Ca^{2+}-imaging to proof an increased neuronal firing.

In contrast, less similarity was found for astroglial (re)activity compared to the other markers. This finding is contrary to previous studies reporting a close relationship between Aβ plaques and reactive astrocytes (Ballweg et al., 2023; Fakhoury, 2018). However, our finding that both, Aβ deposition and MAO-B expression in the thalamus, were significantly elevated in 11.0 months old APPSL70 mice is also reported in previous studies which also found a significant elevation in the hippocampus and cortical structures, though (Ballweg et al., 2023; Olsen et al., 2018). The lack of MAO-B increase in the cortex and hippocampus might be due to the rather early stage of Alzheimer's disease we were capturing in APPSL70 mice without significant neurodegeneration being yet present. Thus, the subcortical activation of astrocytes might be the first step before this astrocytic inflammation is spreading towards other regions of the brain. In that regard, it might be interesting to study the disease time course in amyloidosis mouse models with modulation of microglia and astrocytes at different time points. Thus, one possibility could be to deplete or downregulate microglia or astrocytes, by either using genetically modified animals or administration of specific drugs like pexidartinib (PLX). Another possibility could be to modulate secreted factors of activated microglia, namely interleukin-1α (Il-1α), tumor necrosis factor (TNF), and complement component 1q (C1q), that have been shown to change astrocytes into a reactive and neurotoxic state (Liddelow et al., 2017). However, further studies are needed to evaluate the exact mechanistic relationship between Aβ plaque deposition, astrocytes, microglia, and changes in synaptic density in Alzheimer's disease.

5. Conclusion

Summarizing, we discovered an increase of synaptic density as measured with [^{18}F]UCB-H in an amyloidosis mouse model. This increase is associated with Aβ deposition and microglial inflammation, but not with astrogliosis. Thus, we presume a compensatory mechanism leading to a higher synaptic density in early stages of Alzheimer's disease before the onset of neurodegeneration. Concluding, changes in SV2A expression as measured by [^{18}F]UCB-H PET can provide an useful read-out for the presymptomatic stages of AD and possibly also other neurodegenerative diseases, especially in selecting patients for clinical trials for diagnostic tools and possible treatment options.

Funding

This work was financially supported by F. Hoffmann La Roche AG.

CRediT authorship contribution statement

L.H. Kunze: Writing – original draft, Visualization, Validation, Software, Resources, Methodology, Investigation, Formal analysis, Data curation. **G. Palumbo:** Investigation. **J. Gnörich:** Project administration. **K. Wind-Mark:** Project administration, Investigation. **R. Schaefer:** Writing – review & editing, Investigation. **S. Lindner:** Resources, Project administration. **F.-J. Gildehaus:** Resources, Methodology. **S. Ziegler:** Writing – review & editing, Supervision, Project administration. **M. Brendel:** Writing – review & editing, Supervision, Resources, Project administration, Methodology, Funding acquisition, Conceptualization.

Declaration of competing interest

M.B. has received speaker honoraria from Roche, GE healthcare and Life Molecular Imaging and is an advisor to Life Molecular Imaging. Other than that, the authors declare no conflict of interest.

Acknowledgements

We would like to thank Dr. Lothar Lindemann and the F. Hoffmann La Roche AG for providing the animal model as well as funding for the project.

Supplementary materials

Supplementary material associated with this article can be found, in the online version, at doi:10.1016/j.neuroimage.2025.121165.

Data availability

PET imaging data are available in nifti format and can be transferred per request by the corresponding author. Immunohistochemistry imaging data are available in tif format and can be transferred per request by the corresponding author. Statistics and Graphs are available per request as GraphPad Prism Data.

References

Acioglu, C., Li, L., Elkabes, S., 2021. Contribution of astrocytes to neuropathology of neurodegenerative diseases. Brain Res. 1758, 147291. https://doi.org/10.1016/j.brainres.2021.147291.

Bakhtiari, A., Benedek, K., Law, I., Fagerlund, B., Mortensen, E.L., Osler, M., Lauritzen, M., Larsson, H.B.W., Vestergaard, M.B., 2023. Early cerebral amyloid-β accumulation and hypermetabolism are associated with subtle cognitive deficits before accelerated cerebral atrophy. Geroscience 46 (1), 769–782. https://doi.org/10.1007/s11357-023-01031-w.

Ballweg, A., Klaus, C., Vogler, L., Katzdobler, S., Wind, K., Zatcepin, A., Ziegler, S.I., Secgin, B., Eckenweber, F., Bohr, B., Bernhardt, A., Fietzek, U., Rauchmann, B.-S., Stoecklein, S., Quach, S., Beyer, L., Scheifele, M., Simmet, M., Joseph, E., Brendel, M., 2023. 18F]F-DED PET imaging of reactive astrogliosis in neurodegenerative diseases: preclinical proof of concept and first-in-human data. J. Neuroinflammat. 20 (1), 68. https://doi.org/10.1186/s12974-023-02749-2.

Bartos, L.M., Kunte, S.T., Wagner, S., Beumers, P., Schaefer, R., Zatcepin, A., Li, Y., Griessl, M., Hoermann, L., Wind-Mark, K., Bartenstein, P., Tahirovic, S., Ziegler, S., Brendel, M., Gnörich, J., 2024. Astroglial glucose uptake determines brain FDG-PET alterations and metabolic connectivity during healthy aging in mice. Neuroimage 300, 120860. https://doi.org/10.1016/j.neuroimage.2024.120860.

Bastin, C., Bahri, M.A., Meyer, F., Manard, M., Delhaye, E., Plenevaux, A., Becker, G., Seret, A., Mella, C., Giacomelli, F., Degueldre, C., Balteau, E., Luxen, A., Salmon, E., 2020. In vivo imaging of synaptic loss in Alzheimer's disease with [18F]UCB-H positron emission tomography. Eur. J. Nucl. Med. Mol. Imaging 47 (2), 390–402. https://doi.org/10.1007/s00259-019-04461-x.

Bateman, R.J., Xiong, C., Benzinger, T.L.S., Fagan, A.M., Goate, A., Fox, N.C., Marcus, D. S., Cairns, N.J., Xie, X., Blazey, T.M., Holtzman, D.M., Santacruz, A., Buckles, V., Oliver, A., Moulder, K., Aisen, P.S., Ghetti, B., Klunk, W.E., McDade, E., Morris, J.C., 2012. Clinical and biomarker changes in dominantly inherited Alzheimer's disease. New Eng. J. Med. 367 (9), 795–804. https://doi.org/10.1056/NEJMoa1202753.

Bell, K.F.S., Bennett, D.A., Cuello, A.C., 2007. Paradoxical upregulation of glutamatergic presynaptic boutons during mild cognitive impairment. J. Neurosci. 27 (40), 10810–10817. https://doi.org/10.1523/JNEUROSCI.3269-07.2007.

Bell, K.F.S., de Kort, G.J.L., Steggerda, S., Shigemoto, R., Ribeiro-da-Silva, A., Cuello, A. C., 2003. Structural involvement of the glutamatergic presynaptic boutons in a transgenic mouse model expressing early onset amyloid pathology. Neurosci. Lett. 353, 143–147. https://doi.org/10.1016/j.neulet.2003.09.027.

Benzinger, T.L.S., Blazey, T., Jack, C.R., Koeppe, R.A., Su, Y., Xiong, C., Raichle, M.E., Snyder, A.Z., Ances, B.M., Bateman, R.J., Cairns, N.J., Fagan, A.M., Goate, A., Marcus, D.S., Aisen, P.S., Christensen, J.J., Ercole, L., Hornbeck, R.C., Farrar, A.M., Morris, J.C., 2013. Regional variability of imaging biomarkers in autosomal dominant Alzheimer's disease. Proc. Nat. Acad. Sci. 110 (47). https://doi.org/10.1073/pnas.1317918110.

Blanchard, V., Moussaoui, S., Czech, C., Touchet, N., Bonici, B., Planche, M., Canton, T., Jedidi, I., Gohin, M., Wirths, O., Bayer, T.A., Langui, D., Duyckaerts, C., Tremp, G., Pradier, L., 2003. Time sequence of maturation of dystrophic neurites associated with Aβ deposits in APP/PS1 transgenic mice. Exp. Neurol. 184 (1), 247–263. https://doi.org/10.1016/S0014-4886(03)00252-8.

Blume, T., Focke, C., Peters, F., Deussing, M., Albert, N.L., Lindner, S., Gildehaus, F.-J., von Ungern-Sternberg, B., Ozmen, L., Baumann, K., Bartenstein, P., Rominger, A., Herms, J., Brendel, M., 2018. Microglial response to increasing amyloid load saturates with aging: a longitudinal dual tracer in vivo μpet-study. J. Neuroinflammat. 15 (1), 307. https://doi.org/10.1186/s12974-018-1347-6.

Bolós, M., Llorens-Martín, M., Jurado-Arjona, J., Hernández, F., Rábano, A., Avila, J., 2015. Direct evidence of internalization of tau by microglia In vitro and In vivo. J. Alzheimer's Dis. 50 (1), 77–87. https://doi.org/10.3233/JAD-150704.

Brendel, M., Probst, F., Jaworska, A., Overhoff, F., Korzhova, V., Albert, N.L., Beck, R., Lindner, S., Gildehaus, F.-J., Baumann, K., Bartenstein, P., Kleinberger, G., Haass, C., Herms, J., Rominger, A., 2016. Glial activation and glucose metabolism in a

transgenic amyloid mouse model: a triple-tracer PET study. J. Nuclear Med. 57 (6), 954–960. https://doi.org/10.2967/jnumed.115.167858.
Bretin, F., Bahri, M.A., Bernard, C., Warnock, G., Aerts, J., Mestdagh, N., Buchanan, T., Otoul, C., Koestler, F., Mievis, F., Giacomelli, F., Degueldre, C., Hustinx, R., Luxen, A., Seret, A., Plenevaux, A., Salmon, E., 2015. Biodistribution and radiation dosimetry for the novel SV2A radiotracer [18F]UCB-H: first-in-Human study. Mol. ImAging Biol. 17 (4), 557–564. https://doi.org/10.1007/s11307-014-0820-6.
Bretin, F., Warnock, G., Bahri, M.A., Aerts, J., Mestdagh, N., Buchanan, T., Valade, A., Mievis, F., Giacomelli, F., Lemaire, C., Luxen, A., Salmon, E., Seret, A., Plenevaux, A., 2013. Preclinical radiation dosimetry for the novel SV2A radiotracer [18F]UCB-H. EJNMMI. Res. 3 (1), 35. https://doi.org/10.1186/2191-219X-3-35.
Busche, M.A., Eichhoff, G., Adelsberger, H., Abramowski, D., Wiederhold, K.-H., Haass, C., Staufenbiel, M., Konnerth, A., Garaschuk, O., 2008. Clusters of hyperactive neurons near amyloid plaques in a mouse model of Alzheimer's disease. Science (1979) 321 (5896), 1686–1689. https://doi.org/10.1126/science.1162844.
Chen, M.-K., Mecca, A.P., Naganawa, M., Finnema, S.J., Toyonaga, T., Lin, S., Najafzadeh, S., Ropchan, J., Lu, Y., McDonald, J.W., Michalak, H.R., Nabulsi, N.B., Arnsten, A.F.T., Huang, Y., Carson, R.E., van Dyck, C.H., 2018. Assessing synaptic density in Alzheimer disease with synaptic vesicle glycoprotein 2A positron emission tomographic imaging. JAMa Neurol. 75 (10), 1215–1224. https://doi.org/10.1001/jamaneurol.2018.1836.
Cizeron, M., Qiu, Z., Koniaris, B., Gokhale, R., Komiyama, N.H., Fransén, E., Grant, S.G. N., 2020. A brainwide atlas of synapses across the mouse life span. Science (1979) 369 (6501), 270–275. https://doi.org/10.1126/science.aba3163.
De Wilde, M.C., Overk, C.R., Sijben, J.W., Masliah, E., 2016. Meta-analysis of synaptic pathology in Alzheimer's disease reveals selective molecular vesicular machinery vulnerability. Alzheimer's Dementia 12 (6), 633–644. https://doi.org/10.1016/j.jalz.2015.12.005.
Eckenweber, F., Medina-Luque, J., Blume, T., Sacher, C., Biechele, G., Wind, K., Deussing, M., Briel, N., Lindner, S., Boening, G., von Ungern-Sternberg, B., Unterrainer, M., Albert, N.L., Zwergal, A., Levin, J., Bartenstein, P., Cumming, P., Rominger, A., Höglinger, G.U., Brendel, M., 2020. Longitudinal TSPO expression in tau transgenic P301S mice predicts increased tau accumulation and deteriorated spatial learning. J. Neuroinflammation. 17 (1), 208. https://doi.org/10.1186/s12974-020-01883-5.
Ewers, M., Biechele, G., Suárez-Calvet, M., Sacher, C., Blume, T., Morenas-Rodriguez, E., Deming, Y., Piccio, L., Cruchaga, C., Kleinberger, G., Shaw, L., Trojanowski, J.Q., Herms, J., Dichgans, M., 2020. Higher CSF sTREM2 and microglia activation are associated with slower rates of beta-amyloid accumulation. EMBo Mol. Med. 12 (9). https://doi.org/10.15252/emmm.202012308.
Fakhoury, M., 2018. Microglia and astrocytes in Alzheimer's disease: implications for therapy. Curr. Neuropharmacol. 16 (5), 508–518. https://doi.org/10.2174/1570159X15666170720095240.
Förster, S., Grimmer, T., Miederer, I., Henriksen, G., Yousefi, B.H., Graner, P., Wester, H.-J., Förstl, H., Kurz, A., Dickerson, B.C., Bartenstein, P., Drzezga, A., 2012. Regional expansion of hypometabolism in Alzheimer's disease follows amyloid deposition with temporal delay. Biol. Psychiatry 71 (9), 792–797. https://doi.org/10.1016/j.biopsych.2011.04.023.
Gnörich, J., Koehler, M., Wind-Mark, K., Klaus, C., Zatcepin, A., Palumbo, G., Lalia, M., Sebastian Monasor, L., Beyer, L., Eckenweber, F., Scheifele, M., Gildehaus, F.-J., von Ungern-Sternberg, B., Barthel, H., Sabri, O., Bartenstein, P., Herms, J., Tahirovic, S., Franzmeier, N., Brendel, M., 2024. Towards multicenter β-amyloid PET imaging in mouse models: a triple scanner head-to-head comparison. Neuroimage 297, 120748. https://doi.org/10.1016/j.neuroimage.2024.120748.
Gnörich, J., Reifschneider, A., Wind, K., Zatcepin, A., Kunte, S.T., Beumers, P., Bartos, L. M., Wiedemann, T., Grosch, M., Xiang, X., Fard, M.K., Ruch, F., Werner, G., Koehler, M., Slemann, L., Hummel, S., Briel, N., Blume, T., Shi, Y., Brendel, M., 2023. Depletion and activation of microglia impact metabolic connectivity of the mouse brain. J. Neuroinflammation. 20 (1), 47. https://doi.org/10.1186/s12974-023-02735-8.
Haapasalo, A., Kovacs, D.M., 2011. The many substrates of Presenilin/γ-Secretase. J. Alzheimer's Dis. 25 (1), 3–28. https://doi.org/10.3233/JAD-2011-101065.
Hampel, H., Hardy, J., Blennow, K., Chen, C., Perry, G., Kim, S.H., Villemagne, V.L., Aisen, P., Vendruscolo, M., Iwatsubo, T., Masters, C.L., Cho, M., Lannfelt, L., Cummings, J.L., Vergallo, A., 2021. The amyloid-β pathway in Alzheimer's disease. Mol. Psychiatry 26 (10), 5481–5503. https://doi.org/10.1038/s41380-021-01249-0.
Hickman, S., Allison, E.K., El Khoury, J., 2008. Microglial dysfunction and defective -amyloid clearance pathways in aging Alzheimer's Disease mice. J. Neurosci. 28 (33), 8354–8360. https://doi.org/10.1523/JNEUROSCI.0616-08.2008.
Hickman, S., Izzy, S., Sen, P., Morsett, L., El Khoury, J., 2018. Microglia in neurodegeneration. Nat. Neurosci. 21 (10), 1359–1369. https://doi.org/10.1038/s41593-018-0242-x.
Iaccarino, L., Llibre-Guerra, J.J., McDade, E., Edwards, L., Gordon, B., Benzinger, T., Hassenstab, J., Kramer, J.H., Li, Y., Miller, B.L., Miller, Z., Morris, J.C., Mundada, N., Perrin, R.J., Rosen, H.J., Soleimani-Meigooni, D., Strom, A., Tsoy, E., Wang, G., Rabinovici, G.D., 2024. Molecular neuroimaging in dominantly inherited versus sporadic early-onset Alzheimer's disease. Brain Commun. 6 (3), fcae159. https://doi.org/10.1093/braincomms/fcae159.
Jack, C.R., Knopman, D.S., Jagust, W.J., Shaw, L.M., Aisen, P.S., Weiner, M.W., Petersen, R.C., Trojanowski, J.Q., 2010. Hypothetical model of dynamic biomarkers of the Alzheimer's pathological cascade. Lancet Neurol. 9 (1), 119–128. https://doi.org/10.1016/S1474-4422(09)70299-6.
Janz, R., Goda, Y., Geppert, M., Missler, M., Südhof, T.C., 1999. SV2A and SV2B function as redundant Ca2+ regulators in neurotransmitter release. Neuron 24 (4), 1003–1016. https://doi.org/10.1016/S0896-6273(00)81046-6.
Lichtenthaler, S.F., 2017. Predicting, preventing, and treating Alzheimer's disease. In: Gadebusch Bondio, M., Spöring, F., Gordon, J.-S. (Eds.), Medical ethics, prediction, and prognosis: Interdisciplinary perspectives, 1 ed. Routledge/Taylor & Francis Group, pp. 148–155.
Liddelow, S.A., Guttenplan, K.A., Clarke, L.E., Bennett, F.C., Bohlen, C.J., Schirmer, L., Bennett, M.L., Münch, A.E., Chung, W.-S., Peterson, T.C., Wilton, D.K., Frouin, A., Napier, B.A., Panicker, N., Kumar, M., Buckwalter, M.S., Rowitch, D.H., Dawson, V. L., Dawson, T.M., Barres, B.A., 2017. Neurotoxic reactive astrocytes are induced by activated microglia. Nature 541 (7638), 481–487. https://doi.org/10.1038/nature21029.
Logan, J., Fowler, J.S., Volkow, N.D., Wolf, A.P., Dewey, S.L., Schlyer, D.J., MacGregor, R.R., Hitzemann, R., Bendriem, B., Gatley, S.J., Christman, D.R., 1990. Graphical analysis of reversible radioligand binding from time—Activity measurements applied to [*N*—^{11}C-Methyl]-(−)-cocaine PET studies in Human subjects. J. Cerebral Blood Flow Metabol. 10 (5), 740–747. https://doi.org/10.1038/jcbfm.1990.127.
MATLAB (Version 9.0.0.341360 (R2016a)), 2016. [Computer Software]. The MathWorks Inc. https://www.mathworks.com.
Mecca, A.P., Chen, M., O'Dell, R.S., Naganawa, M., Toyonaga, T., Godek, T.A., Harris, J. E., Bartlett, H.H., Zhao, W., Nabulsi, N.B., Wyk, B.C.V., Varma, P., Arnsten, A.F.T., Huang, Y., Carson, R.E., Dyck, C.H., 2020. In vivo measurement of widespread synaptic loss in Alzheimer's disease with SV2A PET. Alzheimer's Dementia 16 (7), 974–982. https://doi.org/10.1002/alz.12097.
Olsen, M., Aguilar, X., Sehlin, D., Fang, X.T., Antoni, G., Erlandsson, A., Syvänen, S., 2018. Astroglial responses to amyloid-beta progression in a mouse model of Alzheimer's Disease. Mol. ImAging Biol. 20 (4), 605–614. https://doi.org/10.1007/s11307-017-1153-z.
Overhoff, F., Brendel, M., Jaworska, A., Korzhova, V., Delker, A., Probst, F., Focke, C., Gildehaus, F.-J., Carlsen, J., Baumann, K., Haass, C., Bartenstein, P., Herms, J., Rominger, A., 2016. Automated spatial brain normalization and hindbrain white matter reference tissue give improved [18F]-florbetaben PET quantitation in Alzheimer's model mice. Front. Neurosci. 10. https://doi.org/10.3389/fnins.2016.00045.
Palumbo, G., Kunze, L.H., Oos, R., Wind-Mark, K., Lindner, S., Von Ungern-Sternberg, B., Bartenstein, P., Ziegler, S., Brendel, M., 2023. Longitudinal studies on Alzheimer Disease mouse models with multiple tracer PET/CT: application of reduction and refinement principles in daily practice to safeguard animal welfare during progressive aging. Animals 13 (11), 1812. https://doi.org/10.3390/ani13111812.
Rossi, R., Arjmand, S., Bærentzen, S.L., Gjedde, A., Landau, A.M., 2022. Synaptic vesicle glycoprotein 2A: features and functions. Front. Neurosci. 16, 864514. https://doi.org/10.3389/fnins.2022.864514.
Ruch, F., Gnörich, J., Wind, K., Köhler, M., Zatcepin, A., Wiedemann, T., Gildehaus, F.-J., Lindner, S., Boening, G., Von Ungern-Sternberg, B., Beyer, L., Herms, J., Bartenstein, P., Brendel, M., Eckenweber, F., 2024. Validity and value of metabolic connectivity in mouse models of β-amyloid and tauopathy. Neuroimage 286, 120513. https://doi.org/10.1016/j.neuroimage.2024.120513.
Sacher, C., Blume, T., Beyer, L., Biechele, G., Sauerbeck, J., Eckenweber, F., Deussing, M., Focke, C., Parhizkar, S., Lindner, S., Gildehaus, F.-J., von Ungern-Sternberg, B., Baumann, K., Tahirovic, S., Kleinberger, G., Willem, M., Haass, C., Bartenstein, P., Cumming, P., Brendel, M., 2020. Asymmetry of fibrillar plaque burden in amyloid mouse models. J. Nuclear Med. 61 (12), 1825–1831. https://doi.org/10.2967/jnumed.120.242750.
Schindelin, J., Arganda-Carreras, I., Frise, E., Kaynig, V., Longair, M., Pietzsch, T., Preibisch, S., Rueden, C., Saalfeld, S., Schmid, B., Tinevez, J.-Y., White, D.J., Hartenstein, V., Eliceiri, K., Tomancak, P., Cardona, A., 2012. Fiji: an open-source platform for biological-image analysis. Nat. Methods 9 (7), 676–682. https://doi.org/10.1038/nmeth.2019.
Serrano, M.E., Bahri, M.A., Becker, G., Seret, A., Mievis, F., Giacomelli, F., Lemaire, C., Salmon, E., Luxen, A., Plenevaux, A., 2019. Quantification of [18F]UCB-H binding in the rat brain: from kinetic modelling to standardised uptake value. Mol. ImAging Biol. 21 (5), 888–897. https://doi.org/10.1007/s11307-018-1301-0.
Sha, S., Chaigneau, T., Krantic, S., 2023. Pre-symptomatic synaptic dysfunction and longitudinal decay of hippocampal synaptic function in APPPS1 mouse model of Alzheimer's disease is sex-independent. Brain Res. Bull. 198, 36–49. https://doi.org/10.1016/j.brainresbull.2023.04.005.
Snow, A.D., Nochlin, D., Sekiguchi, R., Carlson, S.S., 1996. Identification and immunolocalization of a new class of proteoglycan (Keratan Sulfate) to the neuritic plaques of Alzheimer's Disease. Exp. Neurol. 138, 305–317. https://doi.org/10.1006/exnr.1996.0069.
Spanos, F., Liddelow, S.A., 2020. An overview of astrocyte responses in genetically induced Alzheimer's Disease mouse models. Cells 9 (11), 2415. https://doi.org/10.3390/cells9112415.
Statistical Parametric Mapping (Version 6685), 2016. [Computer Software]. The Wellcome Trust Centre for Neuroimaging, Institute of Neurology, University College London. https://www.fil.ion.ucl.ac.uk/spm/software/spm12/.
Targa Dias Anastacio, H., Matosin, N., Ooi, L., 2022. Neuronal hyperexcitability in Alzheimer's disease: what are the drivers behind this aberrant phenotype? Transl. Psychiatry 12 (1), 257. https://doi.org/10.1038/s41398-022-02024-7.
Terry, R.D., Masliah, E., Salmon, D.P., Butters, N., DeTeresa, R., Hill, R., Hansen, L.A., Katzman, R., 1991. Physical basis of cognitive alterations in alzheimer's disease: synapse loss is the major correlate of cognitive impairment. Ann. Neurol. 30 (4), 572–580. https://doi.org/10.1002/ana.410300410.
Vogler, L., Ballweg, A., Bohr, B., Briel, N., Wind, K., Antons, M., Kunze, L.H., Gnörich, J., Lindner, S., Gildehaus, F.-J., Baumann, K., Bartenstein, P., Boening, G., Ziegler, S.I., Levin, J., Zwergal, A., Höglinger, G.U., Herms, J., Brendel, M., 2023. Assessment of synaptic loss in mouse models of β-amyloid and tau pathology using [18F]UCB-H

PET imaging. NeuroImage: Clin. 39, 103484. https://doi.org/10.1016/j.nicl.2023.103484.
Voytyuk, I., De Strooper, B., Chávez-Gutiérrez, L., 2018. Modulation of γ- and β-secretases as early prevention against Alzheimer's disease. Biol. Psychiatry 83 (4), 320–327. https://doi.org/10.1016/j.biopsych.2017.08.001.
Warnock, G.I., Aerts, J., Bahri, M.A., Bretin, F., Lemaire, C., Giacomelli, F., Mievis, F., Mestdagh, N., Buchanan, T., Valade, A., Mercier, J., Wood, M., Gillard, M., Seret, A., Luxen, A., Salmon, E., Plenevaux, A., 2014. Evaluation of ^{18}F-UCB-H as a novel PET tracer for synaptic vesicle protein 2A in the brain. J. Nuclear Med. 55 (8), 1336–1341. https://doi.org/10.2967/jnumed.113.136143.
Wolf, S.A., Boddeke, H.W.G.M., Kettenmann, H., 2017. Microglia in physiology and disease. Annu. Rev. Physiol. 79 (1), 619–643. https://doi.org/10.1146/annurev-physiol-022516-034406.
Wolfe, M.S., 2021. Probing mechanisms and therapeutic potential of γ-secretase in Alzheimer's disease. Molecules. 26 (2), 388. https://doi.org/10.3390/molecules26020388.
Xu, T., Bajjalieh, S.M., 2001. SV2 modulates the size of the readily releasable pool of secretory vesicles. Nat. Cell Biol. 3 (8), 691–698. https://doi.org/10.1038/35087000.
Zou, K.H., Warfield, S.K., Bharatha, A., Tempany, C.M.C., Kaus, M.R., Haker, S.J., Wells, W.M., Jolesz, F.A., Kikinis, R., 2004. Statistical validation of image segmentation quality based on a spatial overlap index. Acad. Radiol. 11 (2), 178–189. https://doi.org/10.1016/S1076-6332(03)00671-8.